Geophys. J. R. astr. Soc. (1971) **23**, 417–433.

Computation of Synthetic Seismograms with the Reflectivity Method and Comparison with Observations

K. Fuchs and G. Müller

(Received 1971 March 15)*

Summary

The reflectivity method for the computation of synthetic seismograms, as devised by Fuchs, is extended to include the elastic transmission losses and time shifts due to a stack of layers on top of the reflecting medium. Numerical details of this method are described, and a comparison with the ray-theoretical method, as devised by Müller, is given. The results of both methods agree well if the models are not too complicated. The field of application of these methods is the comparison with observed seismograms obtained from refraction studies of the Earth's crust and upper mantle. The reflectivity method is applied to the interpretation of observations along a profile in Central Europe. The compressional velocity of the lower crust beneath this profile increases gradually without showing a pronounced structure. At the Mohorovičić discontinuity whose depth is about 27 km the velocity increases from 6·8 to 8·0 km s^{-1}. The zone immediately below the Moho is homogeneous, followed by an increase in velocity to 8·15 km s^{-1} at a depth of about 35 km.

1. Introduction

During the past few years, it has been emphasized by many seismologists that there is an urgent need to explain not only the kinematic but also the dynamic characteristics of seismic waves. However, as far as explosion seismological investigations of the Earth's crust or upper mantle are concerned, most interpretations are still performed with the aid of travel times or apparent velocities alone, and the amplitudes of arrivals are only tentatively taken into account, if at all. This is caused by the computational difficulties in dealing with the propagation of elastic body waves in currently discussed models of the Earth's crust or upper mantle. If an approximation of such models by homogeneous layers is used, the corresponding computational methods must permit sufficiently fast calculations even in the case of a model with many layers. Only then, the computation of synthetic seismograms can help effectively in the quantitative interpretation of observed seismograms.

Recently, two such methods have been published, the ray-theoretical method and the reflectivity method, as we want to call them in this paper. The ray-theoretical method (Helmberger 1968; Helmberger & Morris 1969, 1970; Müller 1968a, b, 1970, 1971) sums the elementary seismograms corresponding to the primary and multiple rays from the source to the point of observation. In the reflectivity method (Fuchs 1968c, 1970), the numerical integration of the reflectivity (or plane wave reflection

* Received in original form 1970 December 30.

coefficient) of a layered medium is carried out in the horizontal wavenumber or angle of incidence domain. Multiplication with the source spectrum and inverse Fourier transformation yield the seismograms for the displacement components.

In this paper, the reflectivity method as described by Fuchs (1968c) is extended to include the elastic transmission losses and time shifts in a stack of layers on top of the reflecting medium. This is necessary for practical applications of the method, since often only the reflections from the deeper parts of a layered medium, for instance from the crust–mantle boundary are of interest whereas the reflections from the upper parts can be neglected or calculated separately. These deep reflections suffer transmission losses and time shifts in the upper layers which must be taken into account. Furthermore, a comparison of the reflectivity method and the ray-theoretical method is performed for simple layered models, and the advantages and shortcomings of both methods are discussed. Finally, a re-interpretation of a refraction profile in Central Europe will be given. Starting with an earlier travel time interpretation, we could achieve considerable improvements by modelling some of the most prominent amplitude characteristics of the record section of this profile.

2. The reflectivity method

The model for which we want to develop the reflectivity method is shown in Fig. 1. It consists of $n-1$ plane, homogeneous and isotropic layers on top of a half-space which will be termed layer n. The i-th layer is characterized by the P velocity α_i, the S velocity β_i, the density ρ_i and the thickness h_i. We assume an explosive point source in the free surface $z = 0$ without taking into account an interaction, i.e. the compressional wave in layer 1 is spherically symmetric, and no shear and surface waves are excited. We are interested in the compressional reflection from the reflecting zone which comprises the layers $m+1$ through n. The layers 1 through m are assumed to produce only transmission losses and time shifts, both for the P wave propagating downwards from the source to the reflecting zone and for the reflected P wave travelling upwards to the surface. That means that we have to use the exact or generalized ray theory from the depth of the source to the reflecting zone and upwards, and the reflectivity method in its original form (Fuchs 1968c) for the reflection process.

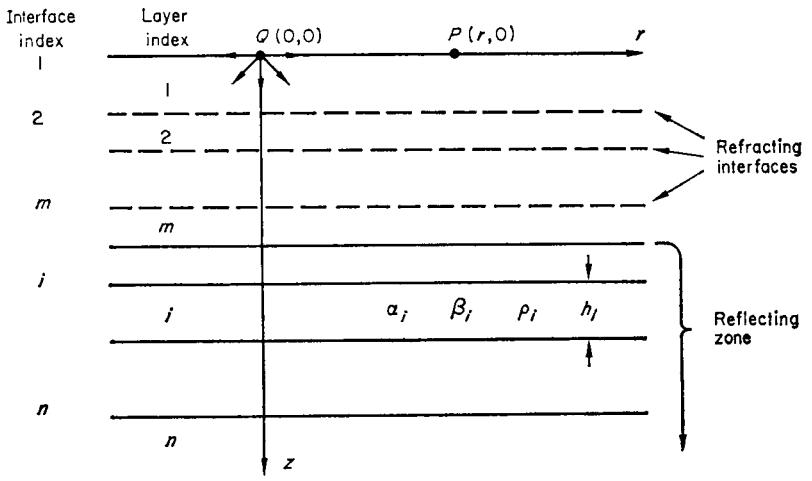

FIG. 1. The layered medium with the explosive point source Q and the point of observation P. The compressional reflection from the reflecting zone suffers elastic transmission losses and time shifts in the layers 1 to m.

The compressional potential of the wave from the explosive point source is

$$\phi_0(r,z,t) = \frac{1}{R} F\left(t - \frac{R}{\alpha_1}\right), \tag{1}$$

where $R^2 = r^2 + z^2$. Its Fourier transform can be written in integral form

$$\bar{\phi}_0(r,z,\omega) = \bar{F}(\omega) \int_0^\infty \frac{k}{jv_1} j_0(kr) \exp(-jv_1 z)\, dk, \tag{2}$$

where $\bar{F}(\omega)$ is the Fourier transform of the excitation function $F(t)$, $Jo(kr)$ the Bessel function of the first kind and order zero, j the imaginary unit, k the horizontal wave number, and

$$v_1 = (k_{\alpha_1}{}^2 - k^2)^{\frac{1}{2}}$$

the vertical wave number ($k_{\alpha_1} = \omega/\alpha_1$).

The next step is to transmit the compressional wave across the interface 2 (see Fig. 1). The resulting Fourier transformed potential of the downgoing P wave in layer 2 has the same form as (2). The integrand includes additionally a transmission coefficient and a second term in the exponential function. This process is continued until layer m is reached. The compressional potential of the P wave in layer m, incident upon the reflecting zone, is

$$\bar{\phi}_1(r,z,\omega) = \bar{F}(\omega) \int_0^\infty \frac{k}{jv_1} j_0(kr)\, P_d(\omega,k) \times \exp\left[-j\left(\sum_{i=1}^{m-1} h_i v_i + \left(z - \sum_{i=1}^{m-1} h_i\right) v_m\right)\right] dk, \tag{3}$$

where $P_d(\omega,k)$ is the product of the transmission coefficients of the interfaces 2, 3, ..., m for a downgoing wave, and

$$v_i = (k_{\alpha_i}{}^2 - k^2)^{\frac{1}{2}},\ v_i' = (k_{\beta_i}{}^2 - k^2)^{\frac{1}{2}} \tag{4}$$

are the vertical wave numbers of compressional waves and shear waves, respectively, in layer i ($k_{\alpha_i} = \omega/\alpha_i$, $k_{\beta_i} = \omega/\beta_i$). Both types of wave numbers occur in $P_d(\omega,k)$. This function and related ones will be given explicitly after the final results have been derived.

The reflection of the incident P wave (3) gives rise to a reflected P wave whose potential in layer m is

$$\bar{\phi}_2(r,z,\omega) = \bar{F}(\omega) \int_0^\infty \frac{k}{jv_1} j_0(kr)\, P_d(\omega,k)\, \bar{R}_{pp}(\omega,k) \times \exp\left[-j\left(\sum_{i=1}^{m} h_i v_i + \left(\sum_{i=1}^{m} h_i - z\right) v_m\right)\right] dk. \tag{5}$$

The complex reflectivity (or plane wave reflection coefficient) $\bar{R}_{pp}(\omega,k)$ of the reflecting zone and its computation have been discussed extensively by Fuchs (1968a, 1971).

The reflected P wave is now transmitted upwards across the interfaces $m, m-1, \ldots, 2$. Its potential in layer 1 is

$$\bar{\phi}_3(r,z,\omega) = \bar{F}(\omega) \int_0^\infty \frac{k}{jv_1} j_0(kr)\, P_d(\omega,k)\, \bar{R}_{pp}(\omega,k)\, P_u(\omega,k) \times \exp\left[-j\left(2\sum_{i=1}^{m} h_i v_i - z v_1\right)\right] dk, \quad (6)$$

where $P_u(\omega, k)$ is the product of the transmission coefficients of the interfaces $2, 3, \ldots, m$ for an upgoing wave.

Our aim is to find the vertical and the horizontal displacement in the free surface $z = 0$. Therefore, the final step is the reflection of the P wave at the free surface. The potential of the reflected P wave is

$$\bar{\phi}_4(r,z.\,\omega) = \bar{F}(\omega) \int_0^\infty \frac{k}{jv_1} j_0(kr)\, P_d(\omega,k)\, \bar{R}_{pp}(\omega,k)\, P_u(\omega,k)\, r_{pp}(\omega,k) \times \exp\left[-j\left(2\sum_{i=1}^{m} h_i v_i + z v_1\right)\right] dk, \quad (7)$$

and the potential of the reflected S wave

$$\bar{\psi}(r,z,\omega) = \bar{F}(\omega) \int_0^\infty \frac{k}{jv_1} j_1(kr)\, P_d(\omega,k)\, \bar{R}_{pp}(\omega,k)\, P_u(\omega,k)\, r_{ps}(\omega,k) \times \exp\left[-j\left(2\sum_{i=1}^{m} h_i v_i + z v_1'\right)\right] dk. \quad (8)$$

In (7) and (8), $r_{pp}(\omega, k)$ and $r_{ps}(\omega, k)$ are the $P-P$ and the $P-S$ reflection coefficient, respectively, of the free surface.

The horizontal and the vertical displacement component in layer 1 are:

$$\bar{u} = \frac{\partial \bar{\phi}_3}{\partial r} + \frac{\partial \bar{\phi}_4}{\partial r} - \frac{\partial \bar{\psi}}{\partial z}$$

$$\bar{w} = \frac{\partial \bar{\phi}_3}{\partial z} + \frac{\partial \bar{\phi}_4}{\partial z} + \frac{\partial \bar{\psi}}{\partial r} + \frac{\bar{\psi}}{r}.$$

For $z = 0$, we get the final result:

$$\bar{u}(r,0,\omega) = \bar{F}(\omega) \int_0^\infty \frac{jk^2}{v_1} j_1(kr)\, P_d\, \bar{R}_{pp}\, P_u \left(1 + r_{pp} - \frac{jv_1'}{k} r_{ps}\right) \times \exp\left(-2j\sum_{i=1}^{m} h_i v_i\right) dk \quad (9)$$

$$\bar{w}(r,0,\omega) = \bar{F}(\omega) \int_0^\infty k j_0(kr)\, P_d\, \bar{R}_{pp}\, P_u \left(1 - r_{pp} + \frac{k}{jv_1} r_{ps}\right) \times \exp\left(-2j\sum_{i=1}^{m} h_i v_i\right) dk \quad (10)$$

The next step is a change of the variable of integration. We choose as new variable the angle γ, related to k by

$$k = (\omega/\alpha_m) \sin\gamma = k_{\alpha_m} \sin\gamma. \tag{11}$$

As long as γ is real, it can be interpreted as the angle of incidence at the top of the reflecting zone.

Introducing the new variable, the functions P_d, P_u, r_{pp} and r_{ps} depend only on γ, and the integrals (9) and (10) are:

$$\bar{u}(r,0,\omega) = \bar{F}(\omega) k_{\alpha_m}^2 \int_{\gamma_1}^{\gamma_2} \sin\gamma \cos\gamma\, j_1(k_{\alpha_m} r \sin\gamma)\, R_{pp}(\omega,\gamma)\, G(\gamma) \times \exp\left(-2jk_{\alpha_m} \sum_{i=1}^{m} h_i \eta_i\right) d\gamma \tag{12}$$

$$\bar{w}(r,0,\omega) = \bar{F}(\omega) k_{\alpha_m}^2 \int_{\gamma_1}^{\gamma_2} \sin\gamma \cos\gamma\, j_0(k_{\alpha_m} r \sin\gamma)\, R_{pp}(\omega,\gamma)\, H(\gamma) \times \exp\left(-2jk_{\alpha_m} \sum_{i=1}^{m} h_i \eta_i\right) d\gamma. \tag{13}$$

The functions $G(\gamma)$ and $H(\gamma)$ are:

$$G(\gamma) = g(\gamma) \prod_{i=2}^{m} T_i(\gamma) \qquad H(\gamma) = h(\gamma) \prod_{i=2}^{m} T_i(\gamma)$$

$$g(\gamma) = 4j \left(\frac{\alpha_m}{\beta_1}\right)^2 \eta_1' \sin\gamma \frac{1}{B} \qquad h(\gamma) = 2 \left(\frac{\alpha_m}{\beta_1}\right)^2 \frac{A}{B}$$

$$A = \left(\frac{\alpha_m}{\beta_1}\right)^2 - 2\sin^2\gamma \qquad B = A^2 + 4\eta_1 \eta_1' \sin^2\gamma$$

$$T_i(\gamma) = 4\rho_{i-1}\rho_i \eta_{i-1}\eta_i \frac{C^2}{D^2}$$

$$C = \eta_i'(d_i \sin^2\gamma - \rho_{i-1}) - \eta_{i-1}'(d_i \sin^2\gamma + \rho_i)$$

$$D = \sin^2\gamma(d_i \sin^2\gamma + \rho_i - \rho_{i-1})^2 + \eta_i \eta_i'(d_i \sin^2\gamma - \rho_{i-1})^2 + \rho_{i-1}\rho_i \eta_i \eta_{i-1}' + \eta_{i-1}[d_i^2 \eta_i \eta_{i-1}' \eta_i' \sin^2\gamma + \eta_{i-1}'(d_i \sin^2\gamma + \rho_i)^2 + \rho_{i-1}\rho_i \eta_i']$$

$$\eta_i = \left[\left(\frac{\alpha_m}{\alpha_i}\right)^2 - \sin^2\gamma\right]^{\frac{1}{2}} \qquad \eta_i' = \left[\left(\frac{\alpha_m}{\beta_i}\right)^2 - \sin^2\gamma\right]^{\frac{1}{2}}$$

$$d_i = 2\left[\rho_{i-1}\left(\frac{\beta_{i-1}}{\alpha_m}\right)^2 - \rho_i\left(\frac{\beta_i}{\alpha_m}\right)^2\right]$$

The displacements at $z = 0$ without the influence of the free surface, i.e. in an infinite half-space instead of layer 1, are found from (12) and (13) by setting

$$g(\gamma) = \frac{j \sin \gamma}{\eta_1} \quad \text{and} \quad h(\gamma) = 1.$$

The limits of integration in (12) and (13) are $\gamma_1 = 0$ and $\gamma_2 = \pi/2 + i\infty$, the path of integration making a right angle at $\gamma = \pi/2$. Integrals of the type (12) and (13) can be computed approximately with the aid of steepest descent or stationary phase methods (Fuchs 1968b, 1971) or by numerical integration (Phinney 1965; Fuchs 1968c). It turns out that it is sufficient for body wave studies to restrict the integration to real angles γ and to choose $\gamma_1 \geqslant 0$ and $\gamma_2 \leqslant \pi/2$. Clarification of this choice and some further details of the numerical methods are discussed in the following.

3. Numerical methods

The most time consuming step in the evaluation of (12) and (13) is the matrix-computation of the reflectivity $R_{pp}(\omega, \gamma)$. This step needs to be done only once, since the reflectivity is the same for all distances r. The circular frequencies ω and the angles γ for which $R_{pp}(\omega, \gamma)$ must be known are found as follows.

In Fig. 2, a reduced travel time diagram for the reflecting zone of an arbitrary model is given. The rectangle drawn in this diagram is, say, the time-distance range for which the synthetic seismograms are to be computed. The length T of the seismograms must be chosen large enough to include all significant arrivals, i.e. the arrivals corresponding to the travel time curve itself and multiply reflected phases from inside the reflecting zone, if their amplitudes are not negligible. Fourier and inverse Fourier transforms are performed with the aid of the fast Fourier transform algorithm (Cooley & Tukey 1965). The frequency interval is $1/T$, and the frequency range extends from 0 to the Nyquist frequency $1/(2\Delta t)$, where Δt is the time sampling interval.

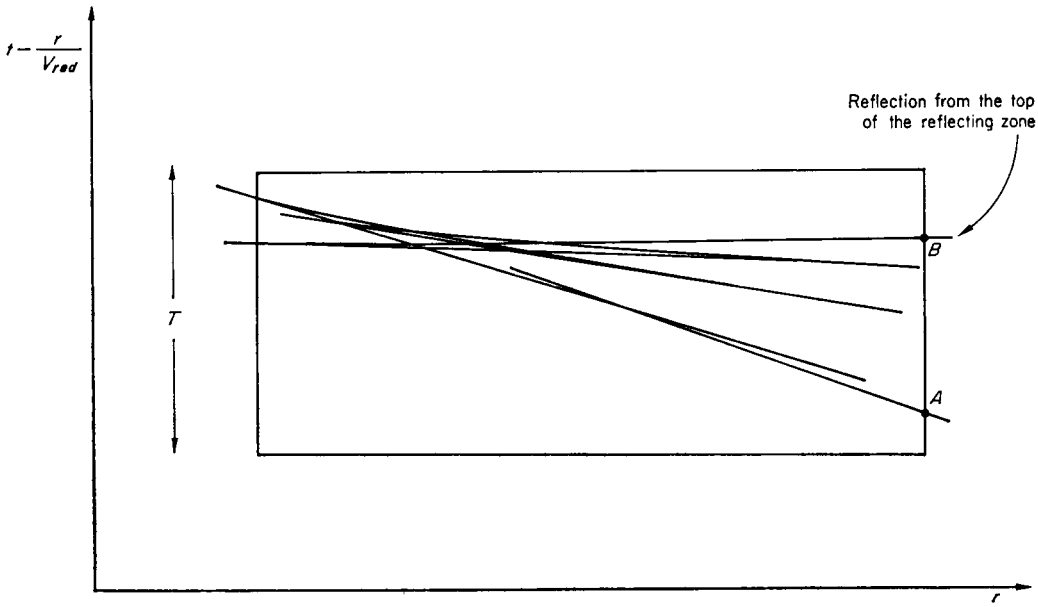

FIG. 2. Reduced travel time diagram for the reflecting zone of an arbitrary model. It is assumed that theoretical seismograms are to be computed inside the rectangle.

However, in most cases this range can be reduced to a more narrow frequency band in which the excitation spectrum $\bar{F}(\omega)$ is essentially different from zero.

The range of angles γ is estimated from the apparent velocities in the time-distance range of interest (Fig. 2). The horizontal wave number k can be related to the apparent velocity c of arrivals at the surface by

$$k = \frac{\omega}{\alpha_m} \sin\gamma = \frac{\omega}{c}.$$

Given the maximum and the minimum value of c, namely c_1 at point A and c_2 at point B, we get the corresponding angles $\gamma_{1,2}$ from

$$\gamma_{1,2} = \arcsin \frac{\alpha_m}{c_{1,2}}. \tag{14}$$

With this choice of γ_2, c_2 cannot be less than the maximum P velocity in the layers overlying the reflecting zone. As a consequence, all radicals η_i and η_i', occurring in the exponential functions of (12) and (13), are real throughout the range of integration. In the usual interpretation of (12) and (13) in terms of superposed plane waves, this means that inhomogeneous plane waves are suppressed.

Since we are mainly interested in applications of the synthetic seismograms to explosion seismological (or refraction) studies, we have replaced the Bessel functions in (12) and (13) by their asymptotic approximations for large arguments:

$$j_0(x) \simeq \sqrt{\left(\frac{2}{\pi x}\right)} \cos\left(x - \frac{\pi}{4}\right) = \frac{1}{\sqrt{2\pi x}} \left\{\exp\left[j\left(x - \frac{\pi}{4}\right)\right] + \exp\left[-j\left(x - \frac{\pi}{4}\right)\right]\right\} \tag{15}$$

$$j_0(x) \simeq \sqrt{\left(\frac{2}{\pi x}\right)} \sin\left(x - \frac{\pi}{4}\right) = \frac{-j}{\sqrt{(2\pi x)}} \left\{\exp\left[j\left(x - \frac{\pi}{4}\right)\right] - \exp\left[-j\left(x - \frac{\pi}{4}\right)\right]\right\} \tag{16}$$

The second exponential term in (15) and (16) corresponds to waves propagating in the positive r-direction (away from the source), whereas the first term describes waves travelling in the negative r-direction (towards the source). At large distances, only the outgoing waves are of physical significance. Stationary phases exist only for the integrals corresponding to these waves (Fuchs 1968b, 1971). The integrals for the incoming waves are negligible, as was shown by numerical evaluation.

The numerical integration is performed either by Simpson's rule or by the trapezoidal rule (Bakun & Eisenberg 1970). We can confirm the statement of these authors that the trapezoidal rule produces much less numerical noise than Simpson's rule. The angle increment in the computations which we have performed up to now varied from 0·1° to 0·5°.

For the time dependence of the explosive point source, we use the derivative of the excitation function $F(t)$ in (1), since the far field displacement of the compressional wave from the source is proportional to this derivative. In our programs, the following analytical form can be chosen:

$$F'(t) = \begin{cases} \sin\delta t - \dfrac{1}{m} \sin m\delta t & 0 \leqslant t \leqslant \tau \\ 0 & t < 0 \text{ and } t > \tau \end{cases} \tag{17}$$

$$\delta = \frac{N\pi}{\tau}, \; m = \frac{N+2}{N}, \; N = 1, 2, 3, \ldots$$

The input parameters are N and the duration τ. This function has N extrema. Therefore, a variety of pulses can be modelled.

4. Comparison with the ray-theoretical method

In this section, both the reflectivity method and the ray-theoretical method (Müller 1970) are applied to a number of models. Such a comparison is desirable since both methods contain approximations. The approximations in the reflectivity method are the restriction to real angles and the use of the asymptotic form of the Bessel functions. The approximations in the ray-theoretical method are the neglection of conversions of the type compressional to shear to compressional and the restriction to certain multiply reflected compressional rays.

For simple *liquid* models, the ray-theoretical computations are exact since all important multiples can be included. Thus, the approximations of the reflectivity method can be checked. An example is given in the left part of Fig. 3 for a model consisting of an intermediate layer between two thick layers. The *solid* version of this model has been investigated by Siskind & Howell (1967) with the aid of model techniques. The unusual density variation follows from correctly modelling this analogue model which consisted of plates of different material and different thickness. The source pulse for the computations followed from (17) for $N = 2$ and

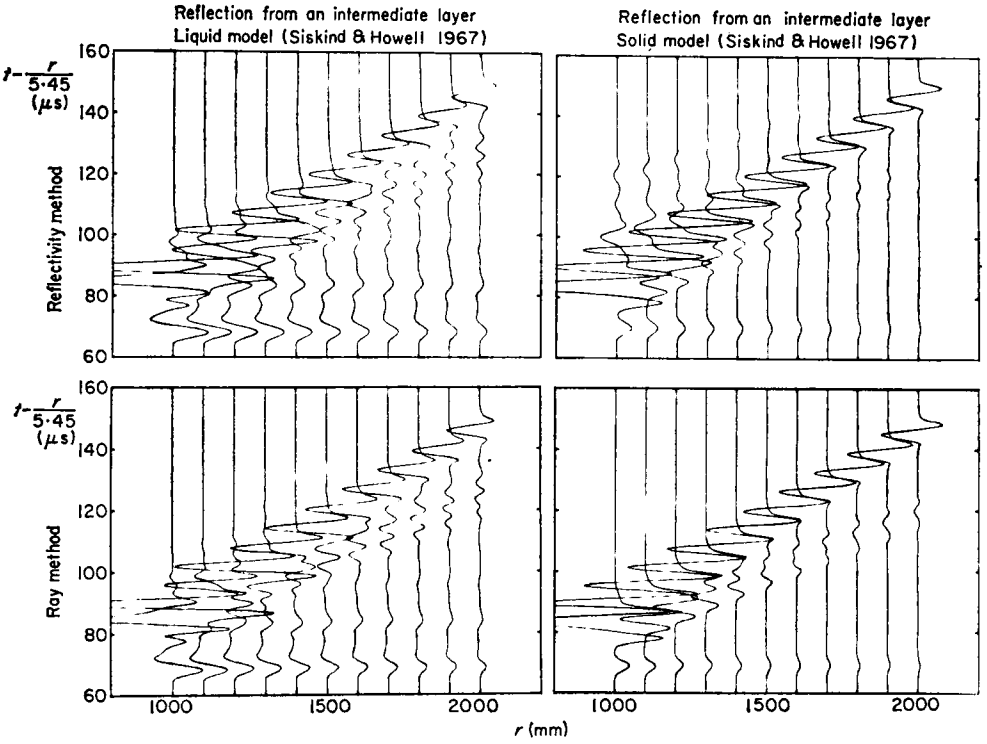

FIG. 3. Comparison of synthetic seismograms, computed with the reflectivity method and the ray-theoretical method. The seismograms on the right side are for a three-dimensional model which was investigated by Siskind & Howell (1967) with the aid of two-dimensional model techniques ($\alpha_1 = 3{\cdot}98$ mm/μsec, $\beta_1 = 2{\cdot}30$ mm/μsec, $\rho_1 = 8{\cdot}92$ g/cm^3, $h_1 = 150$ mm, $\alpha_2 = 4{\cdot}51$, $\beta_2 = 2{\cdot}55$, $\rho_2 = 12{\cdot}85$, $h_2 = 50$, $\alpha_3 = 5{\cdot}45$, $\beta_3 = 3{\cdot}20$, $\rho_3 = 3{\cdot}93$, $h_3 = \infty$). The seismograms on the left side are for the corresponding liquid model. All seismograms represent the vertical displacement at the free surface.

$\tau = 10\,\mu s$. Comparing the seismograms for the liquid model, as computed with the reflectivity method and the ray-theoretical method, we find very good agreement in all parts of the traces. This result is confirmed by computations for other liquid models. Therefore, the approximations of the reflectivity method are justified for investigations of the reflection response from a layered medium.

Applying now both methods to *solid* models, we can check the approximations of the ray-theoretical method, since now the computations with the reflectivity method can be assumed to be exact. The seismograms for the solid Siskind–Howell model (right side of Fig. 3) differ strongly in those parts corresponding to the composite refracted arrival from the intermediate layer. This is due to the neglection of converted waves of the type compressional to shear to compressional in the ray-theoretical computations. The comparatively large amplitudes of these conversions seem to come from the extreme density variations at the boundaries of the intermediate layer. In models with intermediate layers, having constant density throughout, these conversions play only an unimportant role, as can be seen in the example given in Fig. 4.

The only major difference between the seismograms on the left and the right side of Fig. 4 is found near the critical point of the reflection from the upper boundary of the intermediate layer ($r/D = 2{\cdot}67$). The increase in amplitude towards the maximum is more abrupt in the seismogram sections computed with the ray-theoretical method. This is not fully correct. It is due to the fact that in our ray-theoretical programs the elementary seismogram of an arbitrary ray is computed for *line* source excitation in order to save computing time, the reduction to point source excitation being made by multiplication with a constant which is found from a comparison of the wave front approximations for a line source and a point source (Müller 1970). The abrupt increase in the reflection amplitude towards the maximum near the critical point is characteristic of line source excitation (Müller 1971).

In the light of our present experience, we can say the following about the general comparison of the reflectivity method and the ray-theoretical method. The advantage of the reflectivity method lies in the inclusion of multiple reflections and converted waves in the reflecting zone. Therefore the accuracy of the synthetic seismograms is high. Its disadvantage are long computing times, if the reflection response has a long duration. If multiple reflections are disregarded for the moment, this duration is the interval from the first arrival to the reflection from the top of the reflecting zone. It increases with increasing source-receiver distance.

This dependence of the computing time on the length of the seismogram does not exist, if the ray-theoretical method is used. However, in order to avoid prohibitively long computing times in this case it is necessary for more complicated models to omit multiple reflections and conversions. For crustal and upper mantle models, as they are discussed at present, this neglection is often permitted, but for models with stronger velocity and density contrasts it introduces serious errors.

Therefore, we propose to use the ray-theoretical method in order to get an overall picture of the complete refraction profile under investigation, and to use the reflectivity method for detailed studies of special features as, for instance, the amplitude variations along travel time cusps or shadow zones. For upper mantle studies where the Earth's curvature must be taken into account, an Earth-flattening approximation allows the use of both methods in their present form for horizontally layered media (Müller 1971).

5. Application to observations

In this section, some results are presented which were computed in the course of a reinterpretation of the refraction profile Hilders–South in Central Europe. The first travel time interpretation of this profile was made by Fuchs & Landisman (1966).

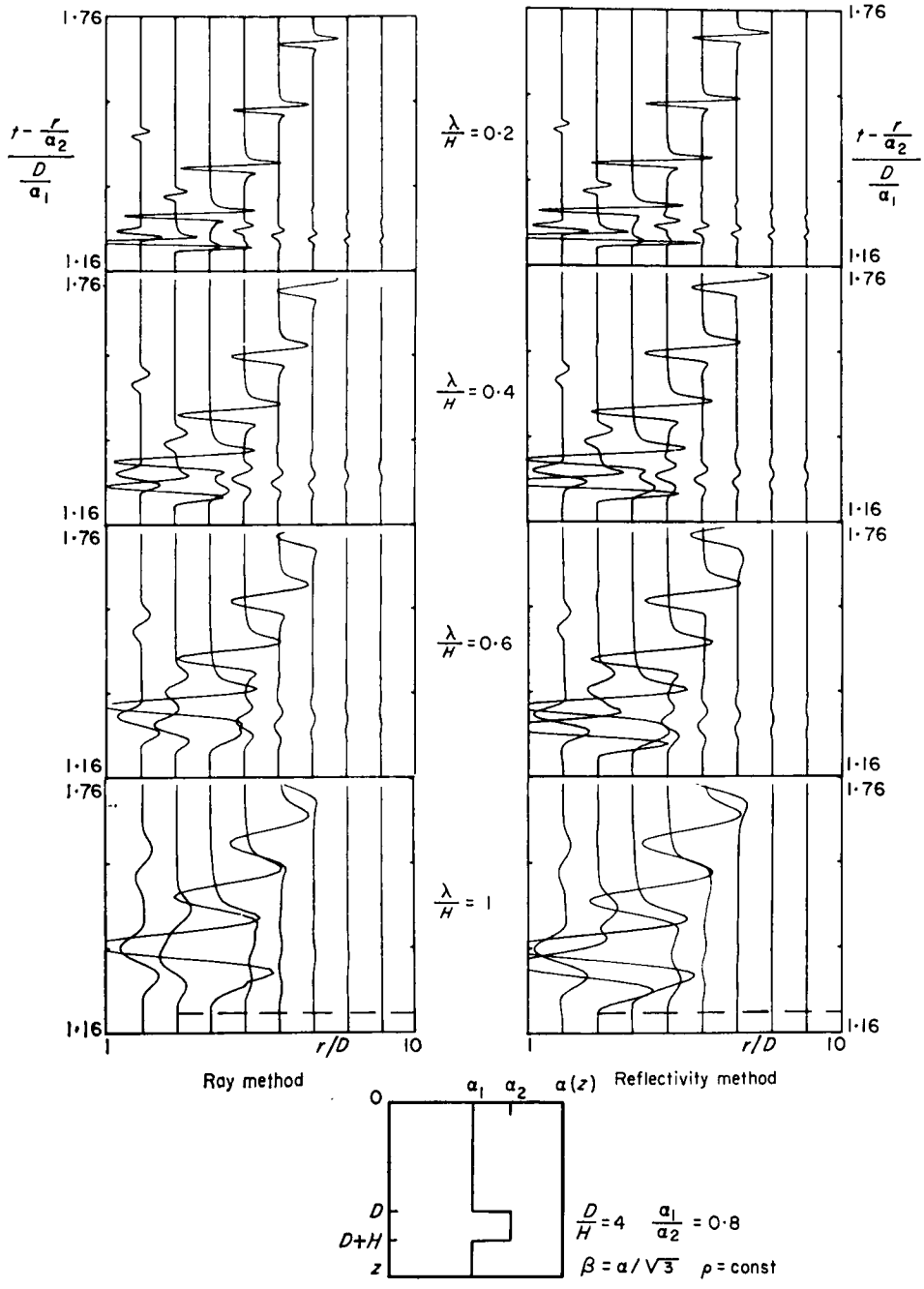

FIG. 4. Comparison of synthetic seismograms, computed with the reflectivity method and the ray-theoretical method. The model is solid and consists of an intermediate layer between two thick layers of the same material. The seismograms are for the vertical displacement in the free surface. λ is the dominant wavelength in the intermediate layer. The seismograms computed with the ray-theoretical method include only compressional multiples.

Fig. 5 shows the observed record section. Although we did not know the magnifications of some of the traces, the instrumental characteristics and the shape of the pulse radiated by the source, we could improve a more recent travel time interpretation of this profile (Kaminski, Fuchs & Menzel 1967) by modelling some of the most prominent amplitude characteristics of the record section. These are firstly due to the Moho reflection P_M, extending from about 60 km to about 190 km, and secondly due to the P_n wave from below the Moho which is visible only beyond 140 km. For the interpretation of the P_n amplitude, we used the amplitude ratio of P_n to the Moho reflection.

We started with the travel time interpretation of Kaminski *et al.* (Fig. 6). The S velocities of this and all other models which we have investigated follow from the P velocities under the assumption that Poisson's ratio is 0·25 throughout the crust. The Nafe–Drake relationship (Talwani, Sutton & Worzel 1959) was used to derive densities from P velocities. Furthermore, the explosive point source is assumed to radiate the pulse which follows from (17) with $N = 2$ and $\tau = 0{\cdot}2$ seconds. Comparing the synthetic with the observed record section, we state the following discrepancies:

(1) There are no clear observed arrivals that could correspond to the strong reflection from the discontinuity at a depth of about 21 km, having a reduced arrival time of about 1 s at the distance 180 km.

(2) The theoretical P_n wave has much too large amplitudes. Especially between 120 and 140 km, where practically no arrivals should occur, the most prominent P_n amplitudes are found in the theoretical section.

Since we were mainly interested in the lower crust and the crust–mantle transition, we improved only those parts of the velocity–depth function below the low velocity zone. When doing this, we tried to keep the model as simple as possible. After some intermediate steps, we found model M3, shown in Fig. 7. It has a constant gradient layer between the low velocity channel and the Moho which lies at a depth of 27 km. There, the jump in velocity is from 6·84 to 8·03 km s^{-1}. Below the Moho, a homogeneous layer of thickness 7 km follows. Finally, there is a transition zone, 2 km thick, with a velocity increase from 8·03 to 8·15 km s^{-1}. This model firstly produces the disappearance of the Moho reflection slightly beyond 180 km. Secondly, the amplitude ratio of P_n to the Moho reflection is very small for distances around 130 km and reaches a value of 1 at a distance between 170 and 180 km. We conclude therefore, that model M3 is able to explain the most prominent features of the observed record section. The most important properties of M3 are the absence of large velocity gradients below the Moho and the simple structure of the lower crust.

There are some arrivals both in Fig. 6 and Fig. 7 which do not line up along travel time branches. They are multiple reflections from inside the reflecting zone. We have not tried to identify all of them. The strongest one, arriving at the reduced time 1 s at the distances from 150 to 180 km in Fig. 7, is a multiple of the refracted wave in the lower crust, reflected at the bottom of the low velocity channel and travelling a second time through the lower crust.

The synthetic seismograms in Figs 6 and 7 were computed with the reflectivity method. Fig. 8 shows a comparison with the results of the ray-theoretical method. The computing time for the seismograms with (without) transmission losses was about 25 per cent (5 per cent) of the computing time with the reflectivity method. The greater speed of the ray-theoretical computation is connected with less accuracy. However, it must be taken into account that the amplitude errors of observed data are often comparable with the discrepancies between the results of the two computational methods.

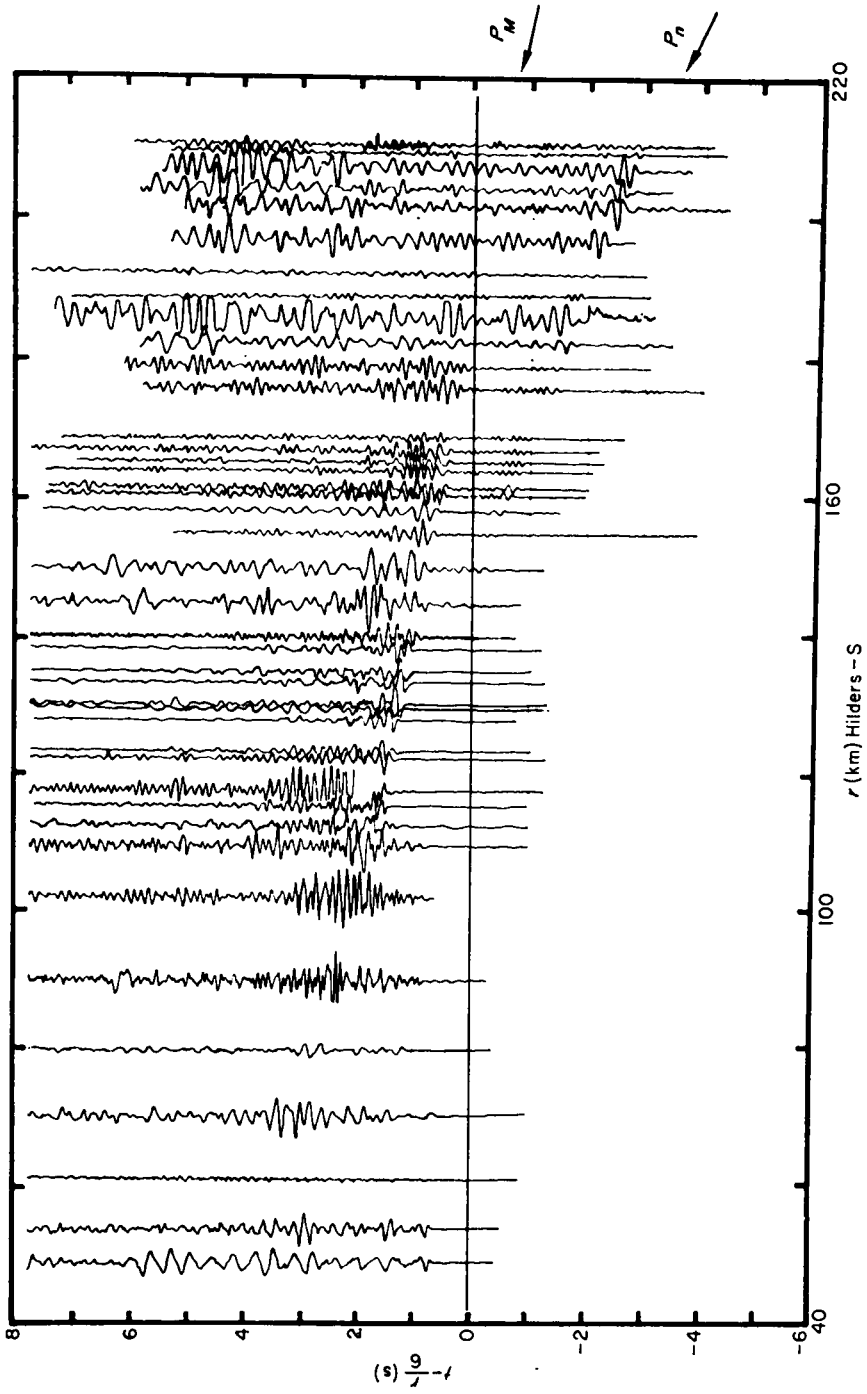

FIG. 5. Record section for the refraction profile Hilders-South in Central Europe (Kaminski, Fuchs & Menzel 1967).

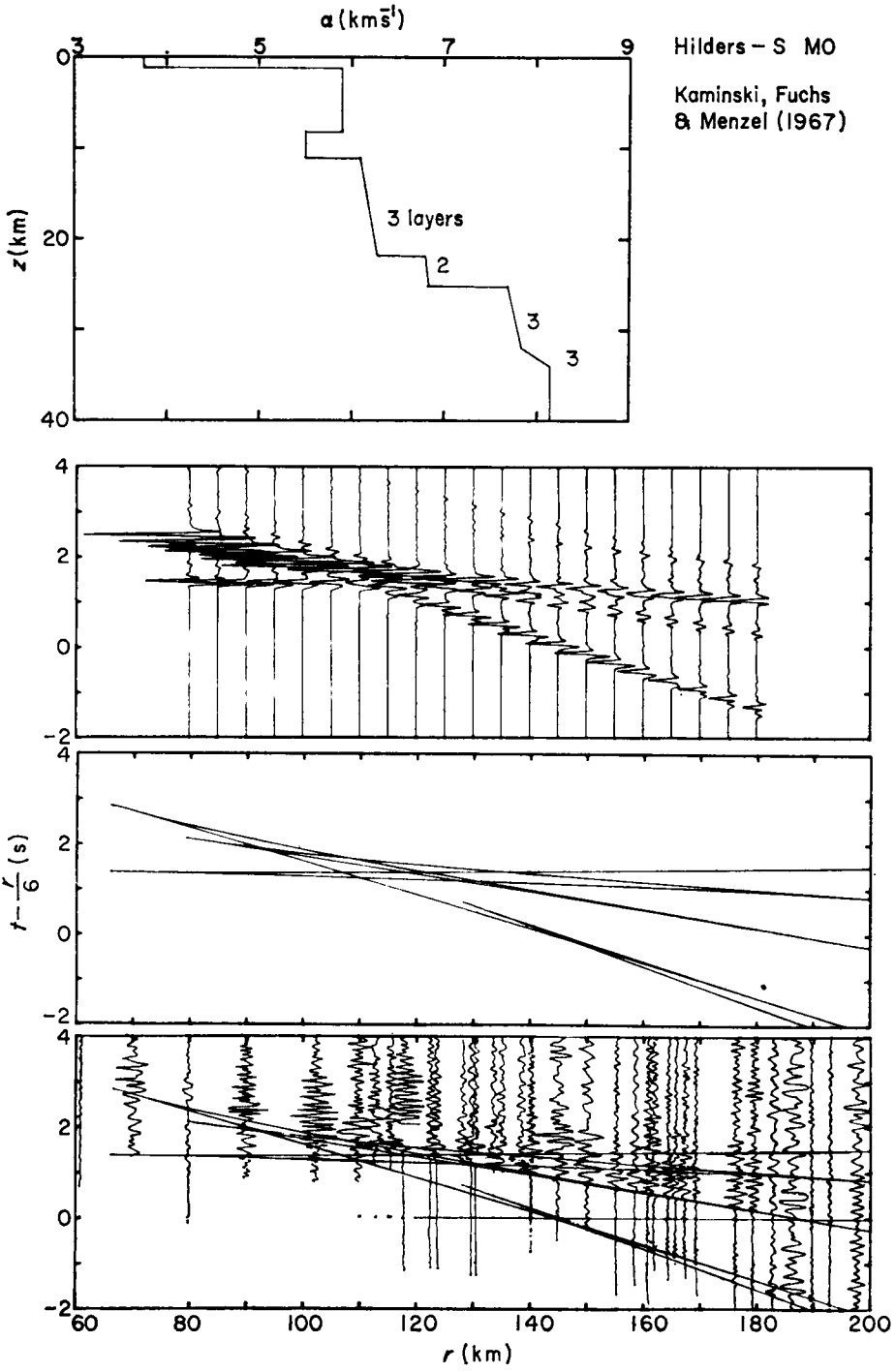

FIG. 6. *P* velocity depth function, synthetic seismogram section (vertical displacement) and travel time curve according to the travel time interpretation of Kaminski, Fuchs & Menzel (1967), compared with the observed record section. The synthetic seismograms and the travel time curve include only the reflection response from the lower boundary of the low velocity channel and the layers below the channel. The numbers near the segments of the velocity-depth function with nonzero velocity gradient are the numbers of homogeneous layers used for the approximation of the corresponding depth range.

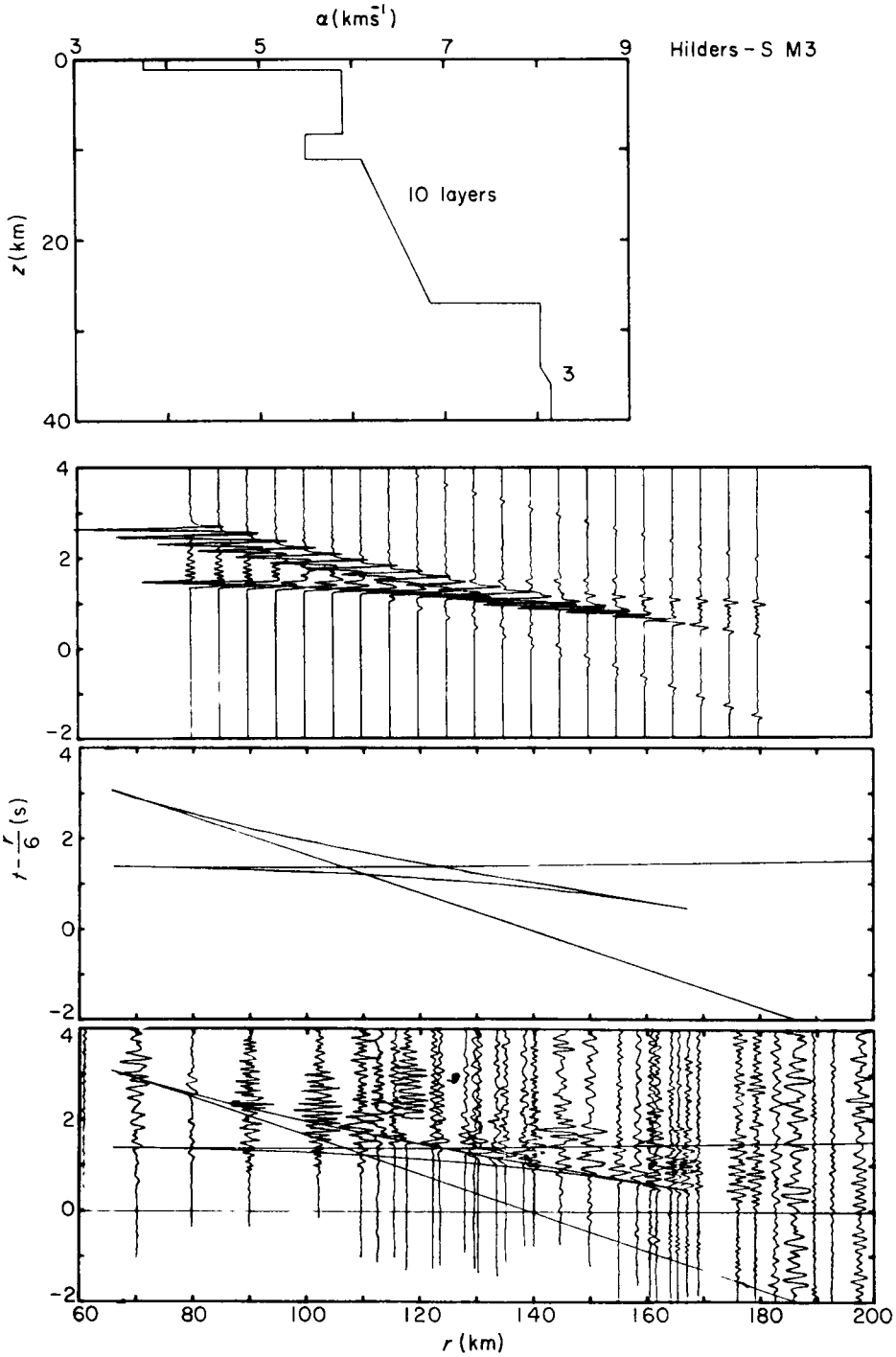

FIG. 7. The same as Fig. 6 for the final model Hilders-S M3.

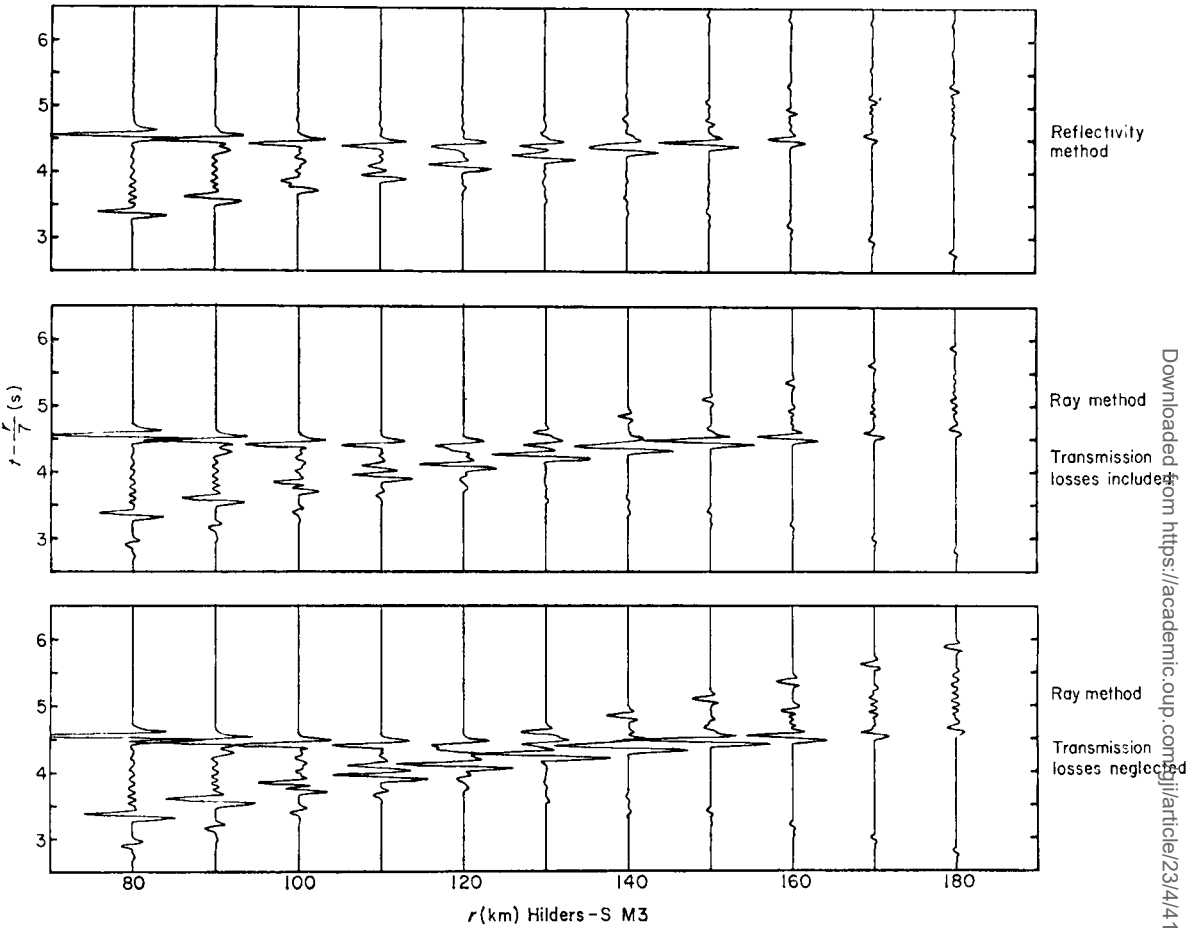

FIG. 8. Synthetic seismograms for model Hilders-S M3, computed with the reflectivity method and the ray-theoretical method. The ray-theoretical seismograms contain only the primary reflections, including those from the upper crust.

6. Conclusions

We arrive at the following conclusions:

(1) The reflectivity method can effectively be used in the quantitative interpretation of explosion seismological observations. The same is true for the ray-theoretical method. In some cases, a combined use will be the optimum interpretational procedure.

(2) The degree to which these new inversion tools can be applied depends strongly on the amplitude information which can be extracted from the observed seismograms. In our present study, for instance, we could not compare directly the amplitudes of neighbouring traces, but only the amplitudes of different arrivals in the same trace. This is a severe restriction of the amplitude information. Therefore, it is an urgent need that instrumental characteristics and actual magnification values be known in future measurements.

(3) Low frequency filtering or low frequency instrumentation is favourable for an interpretation of the records with the aid of synthetic seismograms. In this case, the

noise produced by small scale inhomogeneities will be reduced, and a comparison with synthetic seismograms will be facilitated.

Acknowledgments

We are grateful to our colleagues at the Geophysical Institute, University of Karlsruhe, especially to Professor Stephan Müller, for stimulating and helpful discussions on the subject of this paper. Our research was sponsored by the Deutsche Forschungsgemeinschaft (German Research Association). Computing facilities were made available by the Deutsches Rechenzentrum (German Computing Centre) at Darmstadt, by the Gesellschaft für Kernforschung (Nuclear Research Centre) at Karlsruhe and by the university computing centre at Karlsruhe.

We are indebted to Dr Michael Berry, Seismology Division, Earth Physics Branch, Department of Energy, Mines and Resources, Ottawa, Canada, for valuable discussions during a visit of one of us (K.F.) in 1970.

Geophysical Institute
University of Karlsruhe,
Karlsruhe, West Germany

References

Bakun, W. H. & Eisenberg, A., 1970. Fourier integrals and quadrature-introduced aliasing, *Bull. seism. Soc. Am.*, **60**, 1291.

Cooley, J. W. & Tukey, J. W., 1965. An algorithm for the machine calculation of complex Fourier series, *Math. Computation*, **19**, 297.

Fuchs, K. & Landisman, M., 1966. Detailed crustal investigation along a north-south section through the central part of Western Germany, in: *The Earth beneath the continents*, eds J. S. Steinhart and T. J. Smith, *Monograph No.* 10, *American Geophysical Union, Washington*, 433.

Fuchs, K., 1968a. Das Reflexions- und Transmissionsvermögen eines geschichteten Mediums mit beliebiger Tiefen-Verteilung der elastischen Moduln und der Dichte für schrägen Einfall ebener Wellen, *Z. Geophys.*, **34**, 389.

Fuchs, K., 1968b. Die Reflexion von Kugelwellen an inhomogenen Übergangszonen mit beliebiger Tiefenverteilung der elastischen Moduln und der Dichte, *Habilitationsschrift*, Universität Karlsruhe, 136 p.

Fuchs, K., 1968c. The reflection of spherical waves from transition zones with arbitrary depth-dependent elastic moduli and density, *J. Phys. Earth*, **16**, Special Issue, 27.

Fuchs, K., 1970. On the determination of velocity depth distributions of elastic waves from the dynamic characteristics of the reflected wave field, *Z. Geophys.*, **36**, 531.

Fuchs, K., 1971. The method of stationary phase applied to the reflection of spherical waves from transition zones with arbitrary depth-dependent elastic moduli and density, *Z. Geophys.*, **37**, 89.

Helmberger, D. V., 1968. The crust-mantle transition in the Bering Sea, *Bull. seism.* Soc. Am., **58**, 179.

Helmberger, D. V. & Morris, G. B., 1969. A travel time and amplitude interpretation of a marine refraction profile: primary waves, *J. geophys. Res.*, **74**, 483.

Helmberger, D. V. & Morris, G. B., 1970. A travel time and amplitude interpretation of a marine refraction profile: transformed shear waves, *Bull. seism. Soc. Am.*, **60**, 593.

Kaminski, W., Fuchs, K. & Menzel, H., 1967. *Crustal investigation along a seismic refraction line from the Harz mountains to the Alps*, Paper IASPEI-166, presented at the 14th General Assembly IUGG, Zürich.

Müller, G., 1968a. Theoretical seismograms for some types of point-sources in layered media, Part I: Theory, *Z. Geophys.*, **34,** 15.

Müller, G., 1968b. Theoretical seismograms for some types of point-sources in layered media, Part II: Numerical calculations, *Z. Geophys.*, **34,** 147.

Müller, G., 1970. Exact ray theory and its application to the reflection of elastic waves from vertically inhomogeneous media, *Geophys. J. R. astr. Soc.*, **21,** 261–283.

Müller, G., 1971. Approximate treatment of elastic body waves in media with spherical symmetry, *Geophys. J. R. astr. Soc.* **23,** 435.

Phinney, R. A., 1965. Theoretical calculations of the spectrum of first arrivals in layered elastic mediums, *J. geophys. Res.*, **70,** 5107.

Siskind, D. E. & Howell, B. F., 1967. Scale-model study of refraction arrivals in a three-layered structure, *Bull. seism. Soc. Am.*, **57,** 437.

Talwani, M., Sutton, G. H. & Worzel, J. L., 1959. A crustal section across the Puerto Rico Trench, *J. geophys. Res.*, **64,** 1545.